The Astrophysical Journal, 979:102 (9pp), 2025 February 1 https://doi.org/10.3847/1538-4357/ad9f36

On the Use of Galaxy Catalogs in Gravitational-wave Parameter Estimation

Geoffrey Mo[1,2], Carl-Johan Haster[3,4], and Erik Katsavounidis[1,2]
[1] MIT Kavli Institute for Astrophysics and Space Research, 70 Vassar Street, Cambridge, MA 02139, USA; gmo@mit.edu
[2] MIT LIGO Laboratory, Massachusetts Institute of Technology, 185 Albany Street, Cambridge, MA 02139, USA
[3] Department of Physics and Astronomy, University of Nevada, Las Vegas, 4505 South Maryland Parkway, Las Vegas, NV 89154, USA
[4] Nevada Center for Astrophysics, University of Nevada, Las Vegas, 4505 South Maryland Parkway, Las Vegas, NV 89154, USA
Received 2024 October 18; revised 2024 December 13; accepted 2024 December 13; published 2025 January 21

Abstract

A major challenge in gravitational-wave (GW) multimessenger astrophysics is the imprecise localization of GW compact binary mergers. We investigate the use of a method to include galaxy catalog information in performing parameter estimation of these events. We test its effectiveness with the GW events GW170817, GW190425, and GW190814, as well as with simulated binary neutron star mergers. For GW170817, we recover the true host galaxy as the most probable galaxy after a straightforward mass reweighting, with significantly decreased localization area and volume. On the simulated sample, however, we do not find improvement compared to performing a simple galaxy catalog crossmatch with a regular GW localization. Future investigations into sampling methods may yield improvements that increase the viability of this method.

Unified Astronomy Thesaurus concepts: Gravitational waves (678); Gravitational wave astronomy (675); Neutron stars (1108); Catalogs (205); Compact binary stars (283)

1. Introduction

The observation of gravitational waves (GWs) by the LIGO–Virgo–KAGRA (LVK) Collaboration has become a regular occurrence. This has enabled groundbreaking multimessenger studies of standard siren cosmology (B. P. Abbott et al. 2017a; R. Abbott et al. 2023), neutron star physics (B. P. Abbott et al. 2018), *r*-process nucleosynthesis (J. J. Cowan et al. 2021), binary evolution (K. Belczynski et al. 2018), and general relativity (B. P. Abbott et al. 2019). However, much of this science hinges on the precise and accurate localization of GW events, which remains a challenging problem. Traditionally, most GW localization is performed using Bayesian methods, where an assumption is made that GW sources are distributed following a 3D prior distribution that is isotropic over the sky and uniform in comoving volume. In reality, GW events such as compact-object binary coalescence (CBC) mergers are generally expected to be hosted in galaxies, which are nonuniform and clustered (see e.g., P. J. E. Peebles 1980), suggesting that folding in existing galaxy catalog information directly into localizations can be beneficial.

Galaxy catalogs have most commonly been used with GW data in the context of "dark siren" cosmology (B. F. Schutz 1986; D. E. Holz & S. A. Hughes 2005; M. Fishbach et al. 2019; B. P. Abbott et al. 2021; R. Gray et al. 2023), where GW measurements of luminosity distances for mergers without known host galaxies are combined with statistically inferred redshifts from galaxy catalogs to measure the Hubble constant. In the case of localization of individual GW events, as we discuss here, X. Fan et al. (2014) performed a proof-of-principle analysis in combining GW data with galaxy catalog information. Their method obtains a joint inferred localization through a postprocessing step to regular GW parameter estimation by updating the GW posterior information from a galaxy catalog-informed prior. Other works, including D. J. White et al. (2011), C. Hanna et al. (2014), I. Bartos et al. (2015), N. Gehrels et al. (2016), E. Antolini & J. S. Heyl (2016), L. P. Singer et al. (2016a), and M. C. Artale et al. (2020), have considered the use of galaxy catalogs to optimize searches for electromagnetic (EM) counterparts. These focus on combining the GW-only localization with galaxy catalogs, whereas we here consider using GW and galaxy catalog data simultaneously to produce a localization.

Here, we present a new method that utilizes information about CBC hosts through galaxy catalogs to improve the localization of GW events. The method samples over the known 2D or 3D discrete locations of galaxies during the main GW parameter estimation analysis, in principle allowing for more precise and efficient estimation of each galaxy's probability of being the true CBC host. We have fully implemented it into `Bilby` (G. Ashton et al. 2019; I. M. Romero-Shaw et al. 2020; R. Abbott et al. 2023, 2024), the standard GW parameter estimation tool used by the LVK. We find that our method can significantly reduce localization areas and volumes, especially for nearby GW sources ($\lesssim$250 Mpc) where galaxy catalogs are close to complete. On GW170817, the only GW event with a known host galaxy, our method recovers its host NGC 4993 as the most probable galaxy after a simple mass reweighting. However, when tested on a larger sample of simulated binary neutron star (BNS) mergers, we find no significant improvement on identifying the true hosts compared to crossmatching the normal localization with a galaxy catalog.

The rest of the paper is laid out as follows. In Section 2, we describe our method in detail. We then present its performance on real GW observations and on simulated BNS mergers in Section 3. Finally, we contextualize and discuss our method and describe how it may be improved in Section 4.

2. Method

Our method requires similar inputs to typical GW parameter estimation (GW data, calibration uncertainty envelopes, a set of prior distributions, etc.), with the addition of a galaxy catalog. Its outputs are posteriors both with and without the use of the catalog, a ranked list of galaxies in the localization region, and

for the 3D case, a combined posterior and sky map. The method is outlined as follows:

1. Perform the regular localization for the GW event (i.e., using GW data alone), either with a rapid method such as `BAYESTAR` (L. P. Singer & L. R. Price 2016; L. P. Singer et al. 2016a, 2016b) or with full parameter estimation using, e.g., `Bilby`.
2. Crossmatch the output localization with a galaxy catalog in either a 2D configuration incorporating R.A. and decl. or a 3D configuration, which also includes each galaxy's redshift.
3. Reanalyze the GW data using `Bilby` with the cross-matched galaxy catalog as an input, assuming equal prior weight for each included galaxy. In addition to the typical parameter estimation outputs, this also results in a posterior over each galaxy in the catalog from Step 2.
4. Produce a "combined" localization by sampling over both the usual localization from Step 1 and the output from Step 3, taking into account the completeness of the galaxy catalog at a given distance.

We describe each step in more detail below.

2.1. Step 1: Initial Localization

To reduce the computational cost of sampling over each galaxy in a given catalog, we first compute an initial localization without using information from the galaxy catalog. This allows us to create a "subcatalog" (described in Step 2) that contains only the relevant galaxies, instead of having to sample over the entire galaxy catalog.

The LVK has adopted two main algorithms for the localization of CBC transients: `BAYESTAR` and `Bilby`. `BAYESTAR` is used in low-latency analyses and runs in $\mathcal{O}$ (seconds), whereas `Bilby` is a more computationally expensive method that performs parameter estimation over the full 17-dimensional CBC parameter space. These algorithms (and `Bilby`'s predecessor `LALInference`; J. Veitch et al. 2015) have been shown to produce localizations that are largely similar (L. P. Singer 2014; C. P. L. Berry et al. 2015; B. Farr et al. 2016; G. Ashton et al. 2019; I. M. Romero-Shaw et al. 2020; D. Frostig et al. 2022). In this work, we use `Bilby` to produce our initial localizations to enable the comparison and combination (see Section 2.4) of the resulting sky maps. If latency is a priority (e.g., for rapid EM follow-up of GW events), `BAYESTAR` localizations can be used for this step instead.

2.2. Step 2: Galaxy Catalog Crossmatch

The initial localization produced in Step 1 is then cross-matched with the full galaxy catalog to produce 2D or 3D subcatalogs using the `postprocess.crossmatch` function from `ligo.skymap` (L. P. Singer & L. R. Price 2016; L. P. Singer et al. 2016a, 2016b). This function takes as inputs a GW localization and a list of 2D or 3D coordinates and returns the enclosed area, volume, and probability at each coordinate. Our resulting subcatalog contains the galaxies enclosed in the 99% area (in the 2D case) or volume (3D) of the initial localization.[5]

Throughout this work, we use the NASA/IPAC Extragalactic Database Local Volume Sample (NED-LVS) galaxy catalog (D. O. Cook et al. 2023) as our sample catalog. NED-LVS contains approximately two million galaxies out to a distance of ~1000 Mpc with distance information constructed using data from the NASA/IPAC Extragalactic Database.[6] D. O. Cook et al. (2023) provide an estimate of the NED-LVS completeness at each distance, which is important for assessing the validity of our method as well as for combining the resulting posterior with the initial localization, as described in Step 4.

The crucial difference between the 2D and 3D catalogs is the incorporation of redshift (or distance) information. Since not all galaxy catalogs include redshifts for all their galaxies, we also allow for the use of 2D catalogs that only contain the R.A. and decl. of the galaxies.

We note that our method is largely agnostic to the choice of catalog: if a user wishes to use, e.g., a quasar catalog (such as K. Storey-Fisher et al. 2024) to test the hypothesis that binary black hole (BBH) mergers come from active galactic nuclei (AGN; B. McKernan et al. 2019; M. J. Graham et al. 2020), they may do so. However, the method performs significantly better with redshift information (see Section 3), and combining the initial localization with the catalog-informed localization (Step 4) cannot be performed without an estimate of the catalog completeness at each redshift.

2.3. Step 3: Bilby Analysis with Galaxy Catalog Prior

Using the subcatalog generated in Step 2, we then perform a reanalysis of the GW data utilizing a version of `Bilby` with an additional prior class. First, in order to ensure smooth sampling of the subcatalog by `Bilby`, we sort the galaxies in the subcatalog. We found that a sorting first by redshift or distance (if using a 3D catalog), then R.A., then decl. was sufficiently smooth for `Bilby` to successfully sample over the subcatalog. The subcatalog is passed into `Bilby` as a prior class, and the index of the subcatalog is sampled assuming a uniform prior and subsequently converted to a 2D or 3D coordinate. We use the NED-LVS-specified redshifts, which we then convert to luminosity distances assuming a Planck 2015 cosmology (P. A. R. Ade 2016). To ensure complete and robust sampling coverage of the prior subcatalog, we occasionally had to increase the number of nested sampling live points from 1024 to ~4000. The resulting `Bilby` posterior includes all the usual GW parameters, as well as a posterior indicating the support for each galaxy in the subcatalog.[7]

2.4. Step 4: Combination of the Two Posteriors (Optional)

In the distance regime where galaxy catalogs are close to complete (i.e., within ~250 Mpc; see Figures 10 and 11 of D. O. Cook et al. 2023), the output from Step 3 can be sufficient. However, at larger distances where full catalog completeness can no longer be assumed, we can optionally perform an additional step in combining the initial posterior from Step 1 with the catalog-informed posterior from Step 3. The combination requires the use of a 3D subcatalog and an estimate of the galaxy catalog completeness at each redshift. First, we find the catalog completeness at the redshift of each

[5] This factor is flexible, but we use 99% in this work to ensure a robust subcatalog.

[6] https://ned.ipac.caltech.edu/

[7] The posteriors for R.A., decl., and distance are derived from that of the sampled galaxies.

sample from both the initial and catalog-informed posterior. Then in the catalog-informed posterior, each sample is kept with probability equal to its completeness; the same is done for the initial posterior but with probability (1 − completeness fraction). For example, a sample from the catalog-informed posterior with a distance of 10 Mpc will be kept with probability close to 1, since galaxy catalogs are close to complete at such a distance. On the other hand, a sample from the initial posterior at 1 Gpc, where catalogs are sparse, will be kept with high probability. Then, the two lists of kept samples are combined according to a modified weighting w of each run's evidence:

$$w = \frac{V_{3D}}{V_{init}} \exp(\log \mathcal{Z}_{3D} - \log \mathcal{Z}_{init}), \quad (1)$$

where V_{3D} is the prior volume of the 3D catalog-informed run, represented by the 99% volume of the resulting sky map (as detailed in Step 3); V_{init} is the effective prior volume of the initial run, estimated by finding the comoving volume of the shell between the farthest and nearest values in the distance posterior; and $\mathcal{Z}_{3D}$ and $\mathcal{Z}_{init}$ are the Bayesian evidences from the 3D and initial run, respectively. The combined posterior is then constructed with the kept samples from the 3D run, along with a weight w for the kept samples from the regular run. A probability sky map can then also be produced from the resulting combined posterior.

3. Performance

To evaluate the effectiveness of our method, we tested it on a number of real GW events, as well as on simulated BNS signals. We use the NED-LVS catalog for all of these tests, generating both 2D (where we ignore the redshift information from NED-LVS) and 3D subcatalogs.

3.1. GW170817

The canonical BNS merger GW170817 (B. P. Abbott et al. 2017b, 2017c) is the only GW event with a confirmed host galaxy and is thus a prime test case for our method. Using the `IMRPhenomPv2_NRTidalv2` waveform (M. Hannam et al. 2014; S. Husa et al. 2016; S. Khan et al. 2016; T. Dietrich et al. 2019) implemented using a reduced-order quadrature likelihood (R. Smith et al. 2016; S. Morisaki et al. 2023), we first performed the initial parameter estimation step using the noise-subtracted GW170817 GW strain (R. Abbott et al. 2021) at LIGO Hanford, LIGO Livingston (J. Aasi et al. 2015), and Virgo (F. Acernese et al. 2014; with a low-spin prior and other `Bilby` configurations consistent with GWTC-2.1 R. Abbott et al. 2024 and GWTC-3 R. Abbott et al. 2023). This resulted in a 90% localization area of 14.21 deg^2 and a 90% localization volume of 175.9 Mpc^3. Crossmatching the 99% area and volume localizations to NED-LVS, we find 2460 galaxies in the 2D localization and 44 galaxies in the 3D localization (see Figure 1).

We then performed parameter estimation using our method with both the 2D and 3D subcatalogs. The fractional posterior support for each galaxy in the 2D and 3D subcatalogs is plotted in Figure 1, and the posteriors for the chirp mass, mass ratio, luminosity distance, and the inclination θ_{JN} are shown in Figure 2. NGC 4993, the true host galaxy, is found as the 305th most likely galaxy out of 2460 in the 2D case and as the second most probable of 44 galaxies in the 3D localization volume.

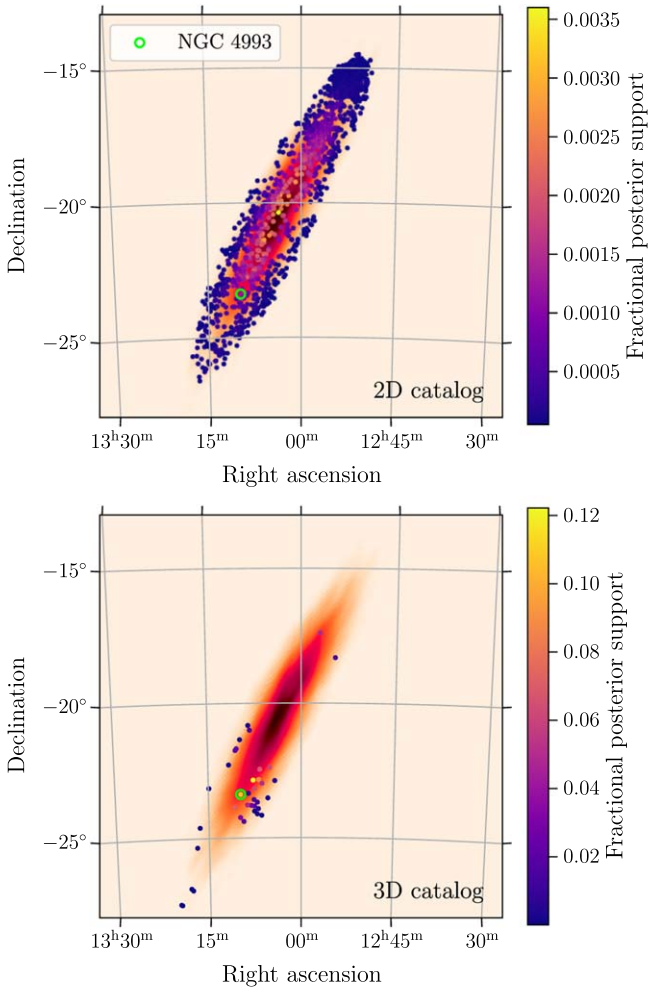

Figure 1. Galaxies in the 2D (top) and 3D (bottom) localization region of GW170817, colored by fractional posterior support as ranked by our method. The true host of GW170817, NGC 4993, is highlighted in the green circle. Of the 2460 NED-LVS galaxies in the 2D 99% localization area of GW170817, NGC 4993 was identified as the 305th most likely galaxy by our method. In the 3D case, our method ranked NGC 4993 as the second most probable of the 44 galaxies in the 3D 99% localization volume. After performing a stellar mass reweighting, NGC 4993 becomes the most probable host in the 3D case (see text).

Due to the density of the galaxies in the 2D localization, much of the area from the initial localization is sampled, leading to similar posteriors from the initial parameter estimation run and the 2D catalog run, as seen for the luminosity distance and inclination in Figure 2. For the 3D subcatalog, where there are only 44 possible galaxies, all with redshift information, there are significant improvements in the luminosity distance and inclination constraints. The luminosity distance of NGC 4993 (using the redshift reported in NED-LVS; G. de Vaucouleurs et al. 1991) is strongly preferred by the 3D catalog run. The inclination constraint is also stronger, with a large overlap with the inclination angle found in B. Abbott et al. (2019) using the GW data in addition to the EM-determined localization and distance. When restricting the posterior samples to only those corresponding to the top four most probable galaxies, this constraint becomes even more robust. While estimates of the extrinsic parameters are improved with our method, Figure 2's left panel shows that intrinsic parameters such as the detector-frame chirp mass M_c and mass ratio q remain unaffected, with essentially identical posteriors across the initial, 2D catalog, and 3D catalog runs. Since all the support for the luminosity

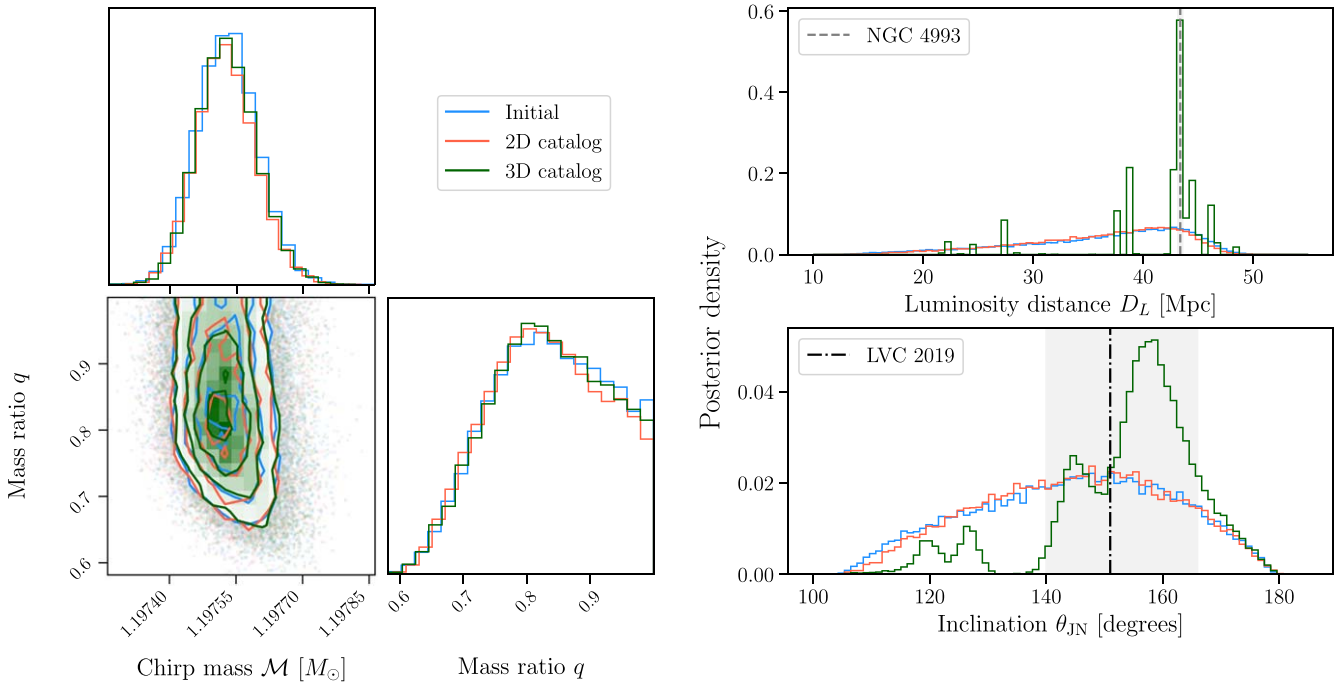

Figure 2. Chirp mass $\mathcal{M}$, mass ratio q, luminosity distance D_L, and inclination $\theta_{\rm JN}$ posteriors for GW170817. The initial (no catalog prior) posteriors are plotted in blue, the 2D catalog posteriors in red, and the 3D catalog posteriors in green. The use of the catalog prior does not change the estimation of the intrinsic parameters such as the chirp mass and mass ratio but improves constraints on extrinsic parameters such as the luminosity distance and inclination angle. For comparison with our posteriors, we show the luminosity distance of NGC 4993 as reported in NED-LVS (G. de Vaucouleurs et al. 1991; D. O. Cook et al. 2023) in the top-right panel; in the bottom-right panel, we show the median and 90% confidence interval estimate of the inclination angle of GW170817 as estimated by the LVC in B. Abbott et al. (2019; low-spin prior, EM-informed result).

distance falls within 60 Mpc, where the NED-LVS galaxy catalog is close to complete, we do not show the combined posteriors as described in Step 4 (Section 2.4); they would overlap almost exactly with the 2D and 3D catalog posteriors.

A summary of the GW170817 localizations is provided in Table 1, showing the dramatic improvement in localization precision and accuracy using our method, especially with a 3D catalog. In the 2D catalog case, the searched area and volume are larger compared to the initial localization, i.e., the pixel/voxel containing NGC 4993 is less probable compared to others in the sky map. This is because, as visible in the top panel of Figure 1, most of the 2460 galaxies in the 2D subcatalog are from two galaxy clusters in the northwest portion of the initial localization. Since there are fewer galaxies in the "middle" of the initial localization, the bulk of the probability is "pushed" to those clusters, away from the true host NGC 4993 in the southeast. The two galaxy clusters are at approximately 200 Mpc, far outside the initial GW170817 distance posterior, and are thus not included in the 3D subcatalog (bottom panel of Figure 1). This is an example of the additional power that a 3D catalog provides compared to the 2D case.

To show the utility of our method for EM follow-up of GW events, we compare our output list of galaxies with those used in the actual search for GW170817's kilonova counterpart. D. A. Coulter et al. (2017) ranked NGC 4993 as the 12th most probable host, while I. Arcavi et al. (2017) found it to be the 5th most probable galaxy, and M. M. Kasliwal et al. (2017) find it as the 3rd most massive galaxy. Our list places NGC 4993 second (10.7% probability), without accounting for stellar mass or luminosity. When then combining that ranking with the stellar mass as estimated in NED-LVS (simply by multiplying each galaxy's fraction of the total mass in the subcatalog with each galaxy's posterior support fraction as computed by our method), NGC 4993 rises to the top as the most probable host for GW170817. We show the top 10 galaxies in this mass-reweighted list in Table 2.

Table 1
GW170817 Localization Statistics

	Initial PE	2D Catalog Prior	3D Catalog Prior
Searched area [deg^2]	5.21	6.86	0.00512
Searched volume [Mpc^3]	60.7	82.9	0.000228
90% area [deg^2]	14.2	10.6	0.898
90% volume [Mpc^3]	176	119	1.54
ln(Bayes factor)	⋯	6.83	8.95

Note. The searched area represents the amount of sky that is ranked as more probable than the true location of the event (and similar for searched volume). The Bayes factor reported is that of each 2D or 3D catalog run compared to the initial PE run.

3.2. GW190425

GW190425 (B. P. Abbott et al. 2020b) was the second BNS merger detected in GWs. Because only two GW detectors were operating at the time of the merger, and because it was located at a much larger distance (~160 Mpc), GW190425's localization (8059 deg^2 90% area) is significantly less precise than that of GW170817. Using its 99% localization area and volume, we created subcatalogs with 815,392 and 144,185 galaxies, respectively. We then applied our method as described above, in the same manner as for GW170817. Even for a localization region as large as this, we found that our method performed well.

Table 2
The 10 Most Probable Galaxies Identified from Our Method, after Mass Reweighting, Using the 3D Catalog for GW170817, GW190425, and GW190814

GW170817						
Rank	Galaxy	R.A.	Decl.	$f_{\rm posterior}$	$f_{\rm mass}$	$f_{\rm posterior} \times f_{\rm mass}$
1	NGC 4993	197.44875	−23.38389	1.06×10^{-1}	5.05×10^{-2}	5.36×10^{-3}
2	ESO 575-G023	193.65467	−18.30828	1.47×10^{-2}	3.03×10^{-1}	4.44×10^{-3}
3	IC 4197	197.01804	−23.79686	2.76×10^{-2}	5.16×10^{-2}	1.42×10^{-3}
4	UGCA 331	197.69142	−23.86575	7.18×10^{-2}	1.81×10^{-2}	1.30×10^{-3}
5	ESO 576-G001	197.59900	−21.68414	2.36×10^{-2}	4.11×10^{-2}	9.73×10^{-4}
6	UGCA 327	196.93696	−22.85786	1.22×10^{-1}	6.41×10^{-3}	7.80×10^{-4}
7	ESO 575-G053	196.27054	−22.38394	6.03×10^{-2}	7.34×10^{-3}	4.43×10^{-4}
8	NGC 4968	196.77492	−23.67703	1.52×10^{-2}	2.86×10^{-2}	4.33×10^{-4}
9	ESO 508-G019	197.46625	−24.23911	3.34×10^{-2}	1.00×10^{-2}	3.35×10^{-4}
10	ESO 575-G055	196.66631	−22.45606	6.98×10^{-2}	3.94×10^{-3}	2.75×10^{-4}
GW190425						
Rank	Galaxy	R.A.	Decl.	$f_{\rm posterior}$	$f_{\rm mass}$	$f_{\rm posterior} \times f_{\rm mass}$
1	CGCG 109-013	246.15412	19.50683	1.27×10^{-4}	6.58×10^{-4}	8.39×10^{-8}
2	NGC 6051	241.23612	23.93269	3.74×10^{-4}	1.53×10^{-4}	5.70×10^{-8}
3	UGC 10160	240.97685	25.01005	3.43×10^{-4}	1.41×10^{-4}	4.84×10^{-8}
4	CGCG 137-028	241.14833	25.18993	3.12×10^{-4}	1.48×10^{-4}	4.61×10^{-8}
5	IC 4569	235.20156	28.29209	3.69×10^{-4}	1.23×10^{-4}	4.56×10^{-8}
6	CGCG 166-030 NED01	235.14696	28.36066	4.00×10^{-4}	1.11×10^{-4}	4.45×10^{-8}
7	IC 4572	235.47580	28.13401	3.87×10^{-4}	1.12×10^{-4}	4.35×10^{-8}
8	IC 0780	184.99324	25.77170	4.00×10^{-4}	1.08×10^{-4}	4.33×10^{-8}
9	NGC 3937	178.17757	20.63131	2.59×10^{-4}	1.60×10^{-4}	4.14×10^{-8}
10	IC 1219	246.11436	19.48257	2.37×10^{-4}	1.72×10^{-4}	4.09×10^{-8}
GW190814						
Rank	Galaxy	R.A.	Decl.	$f_{\rm posterior}$	$f_{\rm mass}$	$f_{\rm posterior} \times f_{\rm mass}$
1	ESO 474-G026	11.78138	−24.37069	1.70×10^{-2}	1.05×10^{-2}	1.79×10^{-4}
2	ESO 474-G041	13.60150	−25.46408	2.07×10^{-2}	5.95×10^{-3}	1.23×10^{-4}
3	WISEA J005034.51-233706.7	12.64375	−23.61853	1.04×10^{-2}	8.34×10^{-3}	8.69×10^{-5}
4	IC 1587	12.18042	−23.56167	7.68×10^{-3}	8.12×10^{-3}	6.24×10^{-5}
5	MCG-04-03-016	12.25621	−23.81136	1.62×10^{-2}	3.16×10^{-3}	5.11×10^{-5}
6	WISEA J004610.38-243900.8	11.54333	−24.65022	1.10×10^{-2}	4.44×10^{-3}	4.88×10^{-5}
7	WISEA J005437.69-250401.8	13.65696	−25.06717	1.76×10^{-2}	2.13×10^{-3}	3.76×10^{-5}
8	WISEA J004842.71-234623.2	12.17825	−23.77306	8.91×10^{-3}	3.81×10^{-3}	3.39×10^{-5}
9	WISEA J004854.94-250410.0	12.22896	−25.06947	2.06×10^{-2}	1.61×10^{-3}	3.31×10^{-5}
10	MCG-04-03-017	12.31121	−23.85850	1.23×10^{-2}	2.67×10^{-3}	3.28×10^{-5}

Note. $f_{\rm posterior}$ is the fraction of total posterior support, assuming the galaxy catalog–informed localization alone. $f_{\rm mass}$ is the fraction of the total mass in the 3D subcatalog in a particular galaxy. $f_{\rm posterior} \times f_{\rm mass}$ is the metric by which we rank the galaxies. Galaxy names, coordinates, and masses are from the NED-LVS catalog (D. O. Cook et al. 2023). Note that in this table, we only present galaxies with mass measurements available in NED-LVS.

The initial, 2D, and 3D catalog sky localizations are shown in Figure 3. Since almost all the probability falls outside of the Galactic plane and within 250 Mpc, we assume a roughly complete catalog and have not combined the initial posterior with the catalog-informed posteriors (Step 4).

Unlike GW170817, there is no known host for GW190425, so it is impossible to assess the correctness of the localization. Nevertheless, as with GW170817, we report the 10 most highly ranked potential hosts from our 3D analysis, after a the mass reweighting described above, in Table 2. These 10 galaxies comprise 2.9% of the total reweighted probability. Since GW190425 is poorly localized, even the most probable galaxies have very little posterior support, indicating that while our method still functions for events with large localizations like GW190425, it is not necessarily as effective as for better-localized events. The 90% areas are 8059, 4086, and 3515 $\deg^2$ for the initial, 2D catalog, and 3D catalog localizations, respectively.

3.3. GW190814

We also test our method with GW190814, a highly asymmetric merger of a 23 $M_\odot$ black hole with a 2.6 $M_\odot$ object that is either a black hole or a neutron star. It was detected by LIGO Hanford, LIGO Livingston, and Virgo, resulting in a 90% localization of 22 $\deg^2$ (R. Abbott et al. 2020).

As with GW170817 and GW190425, we perform initial, 2D, and 3D localizations for GW190814. We show the resulting sky maps for the initial, 3D catalog, and combined (see Section 2.4) initial + 3D catalog localizations in Figure 4 to highlight a scenario where the event's larger distance means that the combined localizations have a meaningful effect. As expected, the combined localization's 90% area (18 $\deg^2$) falls within those of the initial (22 $\deg^2$) and 3D catalog (12 $\deg^2$) localizations.

We also show the initial, 2D catalog, 3D catalog, and the 3D combined posteriors on the luminosity distance, plotted in Figure 5. Due to the large numbers of galaxies (6138) in the 2D

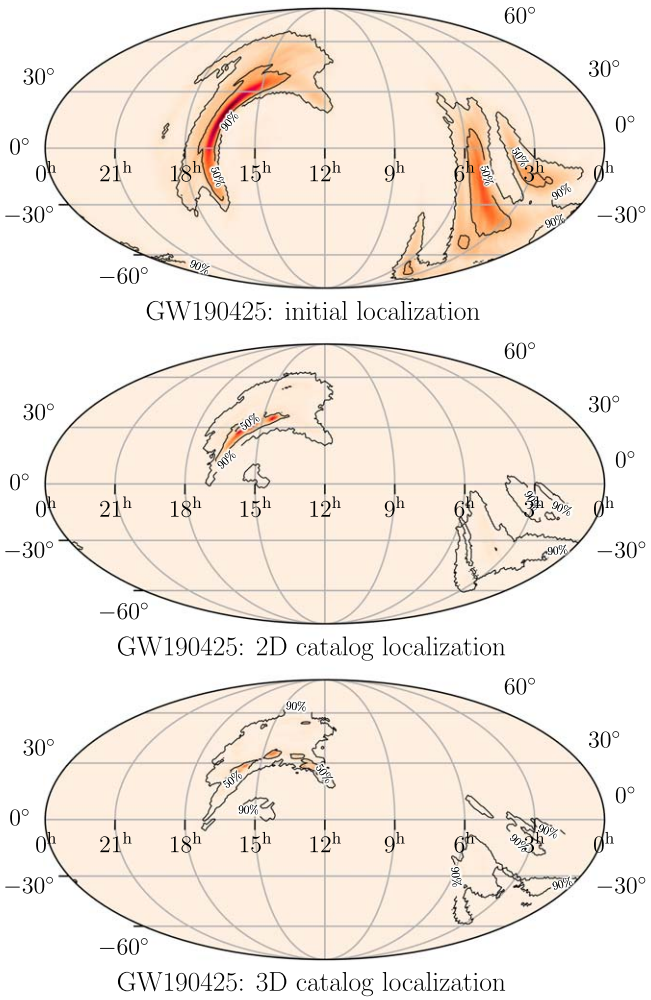

Figure 3. GW190425 initial (top), 2D catalog (center), and 3D (bottom) localizations. Their 90% areas are 8059, 4086, and 3515 deg^2, respectively.

localization, the 2D posterior is not dramatically different from the initial localization. The 3D posterior, using the 836 galaxies in its subcatalog, is much less uniform, showing two distinct modes around 205 and 240 Mpc. When combined with the initial localization, the "peaks" and "valleys" in the posterior become less marked, especially at larger distances, where the NED-LVS completeness falls off.

In addition to the localization, we also produce a ranked list of possible hosts based on the NED-LVS catalog, with the top 10, after a basic mass reweighting, shown in Table 2.

3.4. Performance on Simulated Data

In addition to the real GW events above, we also tested our method on simulated BNS mergers, where we found mixed results. Our simulations consisted of 250 BNS mergers sampled with parameters as described in Table 3 using the `IMRPhenomD` waveform model (S. Husa et al. 2016; S. Khan et al. 2016; S. Morisaki et al. 2023; M. Pürrer et al. 2023) and a network of LIGO Hanford, LIGO Livingston, and Virgo at O4 design sensitivity,[8] simulated in Gaussian noise. We place the simulated mergers at the locations of galaxies in the catalog, enforcing only that a host's *Ks*-band luminosity is greater than 10% of the Milky Way luminosity to avoid potentially clustered low-mass galaxies.[9] We further enforce a network optimal signal-to-noise ratio (S/N) cut of 8 to avoid very poorly localized events. In all, 131 events pass this S/N cut, of which 10 events were removed due to problems with sky map generation from posterior samples (for either the 2D or 3D localizations), resulting in 121 simulated BNS mergers that we analyze below.[10] These simulations are intended to represent a range of realistic BNS detections for which our method is relevant.

Our results are shown as cumulative histograms in Figure 6. As with the events detailed above, we find that our method improves significantly on volume and area localizations compared to regular parameter estimation. In particular, for approximately 10% of our simulated mergers, the simulated true host is within the top 10 ranked galaxies when localized with a 3D catalog. In some cases, the true host is the top ranked galaxy.

However, we found that the crossmatch of the galaxy catalog with the initial parameter estimation localization (ie., Step 2 described in Section 2.2), when sorted by the volume searched probability, performs similarly to our method using a 3D catalog.[11] Since this crossmatch is performed with the sky map, which is generated from a kernel density estimate using a subset of the posterior samples, the resulting probabilities at each galaxy location are, in principle, not as precise estimates of the likelihood compared to our method of sampling directly at the discrete position of each galaxy.[12] In practice, our results show that this discrete sampling does not result in significant improvement. Indeed, for about 13% of our simulated events, the true host was not sampled by `Bilby` when localized with the 3D catalog. This was most prevalent for simulated events at true distances larger than 120 Mpc, where the number of galaxies in the 3D catalog would often be over 10^4.

The improvement in 90% area and 90% volume, while we see no improvement in the distribution of searched galaxies when using a galaxy catalog prior, may seem counterintuitive. This can be explained by the fact that the use of a galaxy catalog prior necessarily restricts the amount of sky area or volume that can be sampled; thus the resulting area or volume can often be smaller than in the case of the initial localization, even when it is not centered on the true host. Essentially, the 90% area and volume are measures of precision, whereas the searched galaxies is a measure of accuracy.

One area where having full posteriors remains advantageous is when considering only the samples corresponding to the most likely few galaxies. We found that this results in a more precise and accurate constraint on the inclination angle $\theta_{\rm JN}$ than using all the samples. This can also be done in the converse: if we obtain some knowledge about the GW inclination angle through the detection of, e.g., a poorly localized short gamma-ray burst counterpart enforcing that $\theta_{\rm JN} \lesssim 30°$, we can further

[8] We use the `aligo_O4high.txt` and `avirgo_O4high_NEW.txt` noise curves from B. P. Abbott et al. (2020a).

[9] This reduces the catalog size from 1.9 million to 1.4 million galaxies, a relatively minor effect.

[10] These 10 events did not show obvious trends in their properties, but we acknowledge that this could result in a ≈8% bias in our cumulative results.

[11] We do not perform a mass or luminosity weighting in using the 3D catalog, only enforcing that hosts have $L_{\rm Ks} > 0.1 L_{\rm MW}$ to match the simulated population.

[12] See, e.g., I. Magaña Hernandez et al. (2024) for a demonstration of the possible variance in distance probability density when estimated from posterior samples using different methods. While this likely has a small effect on our results, it is important to keep in mind for counterpart searches using catalog crossmatches from density-estimated posteriors.

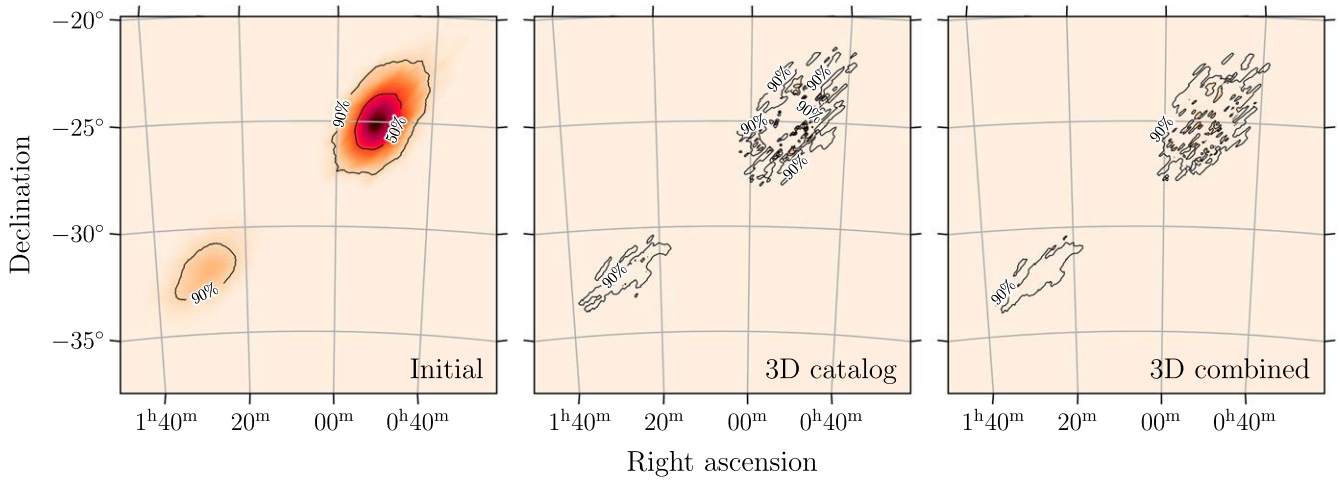

Figure 4. GW190814 initial (left), 3D catalog (center), and combined initial + 3D catalog (right) localizations. Their 90% areas are 22, 12, and 18 deg^2, respectively.

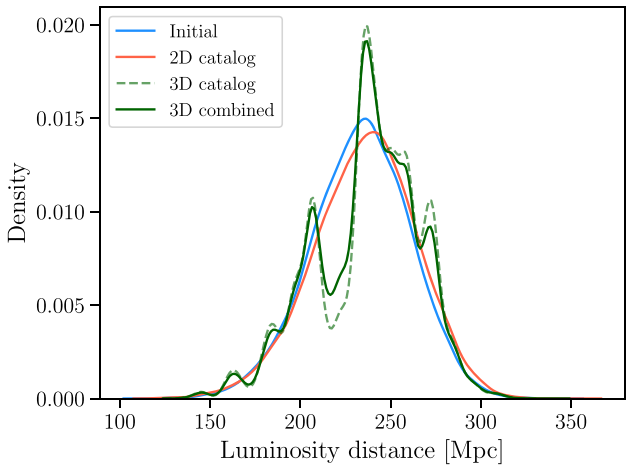

Figure 5. Distance posteriors for GW190814. The initial localization is shown in blue, and the 2D catalog localization is shown in orange. For the 3D catalog localizations, we show the catalog-only localizations in the dashed line and the combined (initial + catalog) localization in the solid line. Note that the agreement between all posteriors is very good at smaller distances, where NED-LVS is complete, and begins to diverge at larger distances.

Table 3
BNS Simulation Parameters

Parameter	Distribution
Chirp mass $\mathcal{M}$	Uniform in components between [1.21, 1.23] $M_\odot$
Mass ratio q	Uniform in components between [0.7, 1.0]
χ_1	Uniform between [0, 0.05]
χ_2	Uniform between [0, 0.05]
$\theta_{\rm JN}$	Uniform in sine
ψ	Uniform between [0, π]
Phase	Uniform between [0, 2π]
Luminosity distance D_L	Galaxies with $D_L < 300$ Mpc, $L_{\rm Ks} > 0.1 L_{\rm MW}$
R.A. and decl.	Galaxies with $D_L < 300$ Mpc, $L_{\rm Ks} > 0.1 L_{\rm MW}$

down-select the list of probable galaxies by only choosing the posterior samples with support at allowed $\theta_{\rm JN}$.

4. Discussion and Conclusion

We have presented a method for using galaxy catalog information in GW parameter estimation. While it showed promise with GW170817, and in principle can provide more precise probabilities for each galaxy being a CBC's host, our simulations concluded that on a population level, it does not outperform simply crossmatching the usual localization with a galaxy catalog. This shortfall is likely due to the often large number of galaxies that must be sampled over. Future work to address different sampling methods, or more sophisticated implementations of galaxy catalog information into parameter estimation tools, may improve the viability of utilizing these important data. In that light, we offer some thoughts on the usage of galaxy catalogs for this purpose.

In this work, we have used NED-LVS (D. O. Cook et al. 2023) as an example galaxy catalog but would like to stress that any galaxy catalog can be used with our method. For example, large composite catalogs like GLADE (G. Dálya et al. 2018) and its successor UpGLADE (M. L. Brozzetti et al. 2024) may extend the utility of our method for mergers at larger distances. Similarly, an AGN catalog such as Quaia (K. Storey-Fisher et al. 2024) could be appropriate for localizing high-mass BBHs, which may reside in AGN disks (B. McKernan et al. 2019; M. J. Graham et al. 2020). Additionally, since our method does not take into account galaxy parameters such as stellar mass, luminosity, or color, observers may reweight the output list of galaxies freely, e.g., to prioritize galaxies with higher masses or luminosities. Beyond searches for EM counterparts where galaxy parameters are among other considerations (including visibility, airmass, etc.), we note that this reweighting must be done carefully to avoid biases in the context of inferring astrophysical parameters (e.g., H_0) from our output galaxies (A. G. Hanselman et al. 2024; G. Perna et al. 2024). Further optimization of host galaxy observing strategies, such as accounting for instrument field of view or networks of telescopes, as discussed by L. P. Singer et al. (2016a) and M. W. Coughlin et al. (2019), are also possible.

The completeness of the input galaxy catalog is one of the most important factors in using this method. Existing catalogs such as NED-LVS begin to fall below 70% K-band completeness at around 350 Mpc ($z \sim 0.075$; D. O. Cook et al. 2023). Current and future surveys such as SDSS-V (J. A. Kollmeier et al. 2017; D. G. York et al. 2000), DESI (DESI Collaboration et al. 2016), LSST at the Vera Rubin Observatory (LSST Science Collaboration et al. 2009; Ž. Ivezić et al 2019), Euclid (R. Laureijs et al. 2011), SPHEREx (O. Doré et al. 2014), and Roman (D. Spergel et al. 2015) will push the forefront of

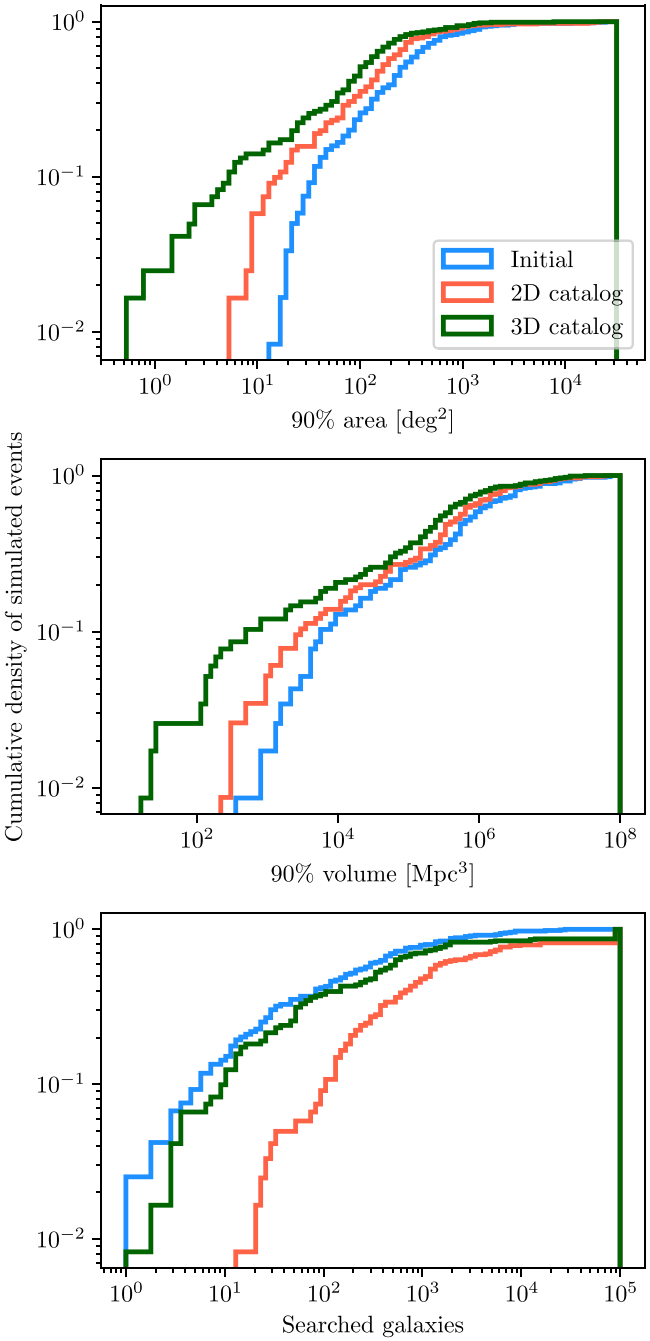

Figure 6. Histograms describing simulated BNS localization performance. Top: cumulative density of the 90% localization areas of our 121 simulated BNS mergers. In blue we show the performance of the "regular" initial localization with a galaxy catalog crossmatch, and in orange and green we show the performance when using a 2D and 3D galaxy catalog, respectively. Middle: cumulative density of the 90% localization volumes of our simulated BNS mergers. Bottom: cumulative density of the number of searched galaxies before arriving at the true simulated host for localizations using 2D (orange) and 3D (green) catalogs. For about 10% of the simulated BNS mergers, both with the regular localization crossmatch and when localized using 3D catalogs, the true host is within the top 10 ranked galaxies.

survey science, ensuring that galaxy catalogs will continue to deepen. Future catalogs may enable the use of our method for mergers at higher redshifts. In a similar vein, powerful upcoming follow-up instruments such as the Vera Rubin Observatory and DSA-2000 (G. Hallinan et al. 2019) might be able to produce on-the-fly galaxy catalogs for a given initial localization, which may be deeper than existing catalogs (B. J. Morsony et al. 2024), enabling an iterative process between GW and EM observers. Also, if this method can be sped up to $\mathcal{O}$ (minute) latencies with further GW parameter estimation improvements, rapid catalog-informed localizations could be useful for compute- and storage-limited radio telescope follow-up (e.g., the Long Wavelength Array; M. M. Anderson et al. 2018), where beamforming on the sky is currently an expensive bottleneck.

A specific region where completeness poses a problem is in the Galactic plane, where extinction complicates observations of galaxies behind the plane at Galactic latitudes $|b| \lesssim 10°$. One way to mitigate this problem for statistical studies of GWs localized with our method is by choosing only the "initial" posterior for $|b| \lesssim 10°$ in the combination step (Step 4 described in Section 2.4). For specific GW events where EM follow-up is the main goal, the impact of the reduction in completeness through the plane is lessened: if deep IR surveys used to construct catalogs are unable to resolve galaxies behind the plane, limitations on observing resources mean that follow-up campaigns on specific events are also unlikely to be able to detect those hosts.

A caveat that may be addressed in future work is in the use of point estimates for galaxy R.A., decl., and redshift from the galaxy catalog. In reality, while 2D coordinate errors are typically small compared to telescope fields of view, redshift uncertainties, especially for photometric redshifts, can be significant. A future improvement to our method may take this into account during sampling by marginalizing over the estimated localization uncertainties.

Beyond follow-up searches for EM counterparts to GW events, improved localizations incorporating galaxy catalogs may also be useful for dark siren cosmology (H.-Y. Chen et al. 2018; M. Soares-Santos et al. 2019; B. P. Abbott et al. 2021), though care must be taken in ensuring consistent cosmological models and in accounting for galaxy redshift uncertainties (C. Turski et al. 2023).

Acknowledgments

We would like to acknowledge useful discussions with Gregg Hallinan, Dave Cook, Sylvia Biscoveanu, Salvatore Vitale, and Leo Singer. G.M. acknowledges the support of the National Science Foundation and the LIGO Laboratory. C.-J.H. acknowledges the support from NASA grant 80NSSC23M0104 and the Nevada Center for Astrophysics. LIGO was constructed by the California Institute of Technology and Massachusetts Institute of Technology with funding from the National Science Foundation and operates under cooperative agreement PHY-0757058. The authors are grateful for computational resources provided by the LIGO Lab and supported by NSF grants PHY-0757058 and PHY-0823459.

This research has made use of data or software obtained from the Gravitational Wave Open Science Center (gwosc.org), a service of the LIGO Scientific Collaboration, the Virgo Collaboration, and KAGRA. This material is based upon work supported by NSF's LIGO Laboratory, which is a major facility fully funded by the National Science Foundation, as well as the Science and Technology Facilities Council (STFC) of the United Kingdom, the Max-Planck-Society (MPS), and the State of Niedersachsen/Germany for support of the construction of Advanced LIGO and construction and operation of the GEO600 detector. Additional support for Advanced LIGO

was provided by the Australian Research Council. Virgo is funded through the European Gravitational Observatory (EGO), by the French Centre National de Recherche Scientifique (CNRS), the Italian Istituto Nazionale di Fisica Nucleare (INFN) and the Dutch Nikhef, with contributions by institutions from Belgium, Germany, Greece, Hungary, Ireland, Japan, Monaco, Poland, Portugal, and Spain. KAGRA is supported by Ministry of Education, Culture, Sports, Science and Technology (MEXT) and Japan Society for the Promotion of Science (JSPS) in Japan; National Research Foundation (NRF) and Ministry of Science and ICT (MSIT) in Korea; and Academia Sinica (AS) and National Science and Technology Council (NSTC) in Taiwan.

This paper carries LIGO document number LIGO-P2400420.

Some of the results in this paper have been derived using the `healpy` (A. Zonca et al. 2019) and `HEALPix` (E. Górski et al. 2005) packages.

Facilities: LIGO, EGO:Virgo, Kamioka:KAGRA.

Software: `astropy` (T. P. Robitaille et al. 2013; A. M. Price-Whelan et al. 2018, 2022), `bilby` (G. Ashton et al. 2019; I. M. Romero-Shaw et al. 2020), `healpy` (A. Zonca et al. 2019), `HEALPix` (E. Górski et al. 2005), `ligo.skymap` (L. P. Singer & L. R. Price 2016; L. P. Singer et al. 2016a, 2016b), `matplotlib` (J. D. Hunter 2007), `numpy` (C. R. Harris et al. 2020), `pandas` (W. McKinney 2010; pandas development team 2020), `pesummary` (C. Hoy & V. Raymond 2021).

ORCID iDs

Geoffrey Mo https://orcid.org/0000-0001-6331-112X
Carl-Johan Haster https://orcid.org/0000-0001-8040-9807

References

Aasi, J., Abbott, B. P., Abbott, R., et al. 2015, CQGra, 32, 074001
Abbott, B., Abbott, R., Abbott, T., et al. 2019, PhRvX, 9, 011001
Abbott, B. P., Abbott, R., Abbott, T. D., et al. 2020a, Noise Curves used for Simulations in the Update of the Observing Scenarios Paper, https://dcc.ligo.org/LIGO-T2000012/public
Abbott, B. P., Abbott, R., Abbott, T. D., et al. 2017a, Natur, 551, 85
Abbott, B. P., Abbott, R., Abbott, T. D., et al. 2017b, PhRvL, 119, 161101
Abbott, B. P., Abbott, R., Abbott, T. D., et al. 2017c, ApJL, 848, L12
Abbott, B. P., Abbott, R., Abbott, T. D., et al. 2018, PhRvL, 121, 161101
Abbott, B. P., Abbott, R., Abbott, T. D., et al. 2019, PhRvL, 123, 011102
Abbott, B. P., Abbott, R., Abbott, T. D., et al. 2020b, ApJL, 892, L3
Abbott, B. P., Abbott, R., Abbott, T. D., et al. 2021, ApJ, 909, 218
Abbott, R., Abbott, T. D., Abraham, S., et al. 2020, ApJL, 896, L44
Abbott, R., Abbott, T. D., Abraham, S., et al. 2021, SoftX, 13, 100658
Abbott, R., Abe, H., Acernese, F., et al. 2023, ApJ, 949, 76
Abbott, R., Abbott, T. D., Acernese, F., et al. 2023, PhRvX, 13, 041039
Abbott, R., Abbott, T. D., Acernese, F., et al. 2024, PhRvD, 109, 022001
Acernese, F., Agathos, M., Agatsuma, K., et al. 2014, CQGra, 32, 024001
Ade, P. A. R., et al. 2016, A&A, 594, A13
Anderson, M. M., Hallinan, G., Eastwood, M. W., et al. 2018, ApJ, 864, 22
Antolini, E., & Heyl, J. S. 2016, MNRAS, 462, 1085
Arcavi, I., Hosseinzadeh, G., Howell, D. A., et al. 2017, Natur, 551, 64
Artale, M. C., Bouffanais, Y., Mapelli, M., et al. 2020, MNRAS, 495, 1841
Ashton, G., Hbner, M., Lasky, P. D., et al. 2019, ApJS, 241, 27
Bartos, I., Crotts, A. P. S., & Márka, S. 2015, ApJL, 801, L1
Belczynski, K., Askar, A., Arca-Sedda, M., et al. 2018, A&A, 615, A91
Berry, C. P. L., Mandel, I., Middleton, H., et al. 2015, ApJ, 804, 114
Brozzetti, M. L., Dálya, G., Greco, G., et al. 2024, A&A, 684, A44
Chen, H.-Y., Fishbach, M., & Holz, D. E. 2018, Natur, 562, 545
Cook, D. O., Mazzarella, J. M., Helou, G., et al. 2023, ApJS, 268, 14
Coughlin, M. W., Antier, S., Corre, D., et al. 2019, MNRAS, 489, 5775
Coulter, D. A., Foley, R. J., Kilpatrick, C. D., et al. 2017, Sci, 358, 1556
Cowan, J. J., Sneden, C., Lawler, J. E., et al. 2021, RvMP, 93, 015002
Dálya, G., Galgóczi, G., Dobos, L., et al. 2018, MNRAS, 479, 2374
de Vaucouleurs, G., de Vaucouleurs, A., Corwin, H. G. J., et al. 1991, Third Reference Catalogue of Bright Galaxies (New York: Springer)
DESI Collaboration, Aghamousa, A., Aguilar, J., et al. 2016, arXiv:1611.00036
Dietrich, T., Samajdar, A., Khan, S., et al. 2019, PhRvD, 100, 044003
Doré, O., Bock, J., Ashby, M., et al. 2014, arXiv:1412.4872
Fan, X., Messenger, C., & Heng, I. S. 2014, ApJ, 795, 43
Farr, B., Berry, C. P. L., Farr, W. M., et al. 2016, ApJ, 825, 116
Fishbach, M., Gray, R., Magaña Hernandez, I., et al. 2019, ApJL, 871, L13
Frostig, D., Biscoveanu, S., Mo, G., et al. 2022, ApJ, 926, 152
Gehrels, N., Cannizzo, J. K., Kanner, J., et al. 2016, ApJ, 820, 136
Górski, K. M., Hivon, E., Banday, A. J., et al. 2005, ApJ, 622, 759
Graham, M. J., Ford, K. E. S., McKernan, B., et al. 2020, PhRvL, 124, 251102
Gray, R., Beirnaert, F., Karathanasis, C., et al. 2023, JCAP, 12, 023
Hallinan, G., Ravi, V., Weinreb, S., et al. 2019, BAAS, 51, 255
Hanna, C., Mandel, I., & Vousden, W. 2014, ApJ, 784, 8
Hannam, M., Schmidt, P., Bohé, A., et al. 2014, PhRvL, 113, 151101
Hanselman, A. G., Vijaykumar, A., Fishbach, M., & Holz, D. E. 2024, arXiv:2405.14818
Harris, C. R., Millman, K. J., van der Walt, S. J., et al. 2020, Natur, 585, 357
Holz, D. E., & Hughes, S. A. 2005, ApJ, 629, 15
Hoy, C., & Raymond, V. 2021, SoftX, 15, 100765
Hunter, J. D. 2007, CSE, 9, 90
Husa, S., Khan, S., Hannam, M., et al. 2016, PhRvD, 93, 044006
Ivezić, Ž., Kahn, S. M., Tyson, J. A., et al. 2019, ApJ, 873, 111
Kasliwal, M. M., Nakar, E., Singer, L. P., et al. 2017, Sci, 358, 1559
Khan, S., Husa, S., Hannam, M., et al. 2016, PhRvD, 93, 044007
Kollmeier, J. A., Zasowski, G., Rix, H.-W., et al. 2017, arXiv:1711.03234
Laureijs, R., Amiaux, J., Arduini, S., et al. 2011, arXiv:1110.3193
LSST Science Collaboration, Abell, P. A., Allison, J., et al. 2009, arXiv:0912.0201
Magaña Hernandez, I., d'Emilio, V., Morisaki, S., Bhardwaj, M., & Palmese, A. 2024, ApJL, 971, L5
McKernan, B., Ford, K. E. S., Bartos, I., et al. 2019, ApJL, 884, L50
McKinney, W. 2010, in Proc. 9th Python in Science Conference, ed. S. van der Walt & J. Millman (SciPy), 56, https://proceedings.scipy.org/articles/Majora-92bf1922-00a
Morisaki, S., Smith, R., Tsukada, L., et al. 2023, PhRvD, 108, 123040
Morsony, B. J., De Los Santos, R., Hernandez, R., et al. 2024, MNRAS, 533, 510
pandas development team 2020, pandas-dev/pandas: Pandas, v2.2.2, Zenodo, doi:10.5281/zenodo.3509134
Peebles, P. J. E. 1980, The Large-scale Structure of the Universe (Princeton, NJ: Princeton Univ. Press)
Perna, G., Mastrogiovanni, S., & Ricciardone, A. 2024, arXiv:2405.07904
Price-Whelan, A. M., Sipőcz, B. M., Günther, H. M., et al. 2018, AJ, 156, 123
Price-Whelan, A. M., Lim, P. L., Earl, N., et al. 2022, ApJ, 935, 167
Pürrer, M., Khan, S., Ohme, F., Birnholtz, O., & London, L. 2023, IMRPhenomD: Phenomenological waveform model, Astrophysics Source Code Library, ascl:2307.019
Robitaille, T. P., Tollerud, E. J., Greenfield, P., et al. 2013, A&A, 558, A33
Romero-Shaw, I. M., Talbot, C., Biscoveanu, S., et al. 2020, MNRAS, 499, 3295
Schutz, B. F. 1986, Natur, 323, 310
Singer, L. P., Chen, H.-Y., Holz, D. E., et al. 2016a, ApJL, 829, L15
Singer, L. P., Chen, H.-Y., Holz, D. E., et al. 2016b, ApJS, 226, 10
Singer, L. P., & Price, L. R. 2016, PhRvD, 93, 024013
Singer, L. P., et al. 2014, ApJ, 795, 105
Smith, R., Field, S. E., Blackburn, K., et al. 2016, PhRvD, 94, 044031
Soares-Santos, M., Palmese, A., Hartley, W., et al. 2019, ApJL, 876, L7
Spergel, D., Gehrels, N., Baltay, C., et al. 2015, arXiv:1503.03757
Storey-Fisher, K., Hogg, D. W., Rix, H.-W., et al. 2024, ApJ, 964, 69
Turski, C., Bilicki, M., Dálya, G., Gray, R., & Ghosh, A. 2023, MNRAS, 526, 6224
Veitch, J., Raymond, V., Farr, B., et al. 2015, PhRvD, 91, 042003
White, D. J., Daw, E. J., & Dhillon, V. S. 2011, CQGra, 28, 085016
York, D. G., Adelman, J., Anderson, J. E. J., et al. 2000, AJ, 120, 1579
Zonca, A., Singer, L., Lenz, D., et al. 2019, JOSS, 4, 1298